



## The effects of topology upon fluid-flow and heat-transfer within cellular copper structures

J. Tian <sup>a</sup>, T. Kim <sup>a</sup>, T.J. Lu <sup>a,\*</sup>, H.P. Hodson <sup>a</sup>, D.T. Queheillalt <sup>b</sup>,  
H.N.G. Wadley <sup>b</sup>

<sup>a</sup> Department of Engineering, University of Cambridge, Trumpington Street, Cambridge CB2 1PZ, UK

<sup>b</sup> Materials Science Department, School of Engineering and Applied Sciences, University of Virginia, Charlottesville, VA 22903, USA

Received 19 September 2002

### Abstract

The fluid-flow and heat-transfer features of cellular metal lattice structures made from copper by transient liquid phase (TLP) bonding and brazing of plane weave copper meshes (screens) were experimentally characterized under steady-state forced air convection. Due to the inherent structural anisotropy of this metal textile derived structure, the characterizations were performed for several configurations to identify the preferable orientation for maximizing thermal performance as a heat dissipation medium. Results show that the friction factor of bonded wire screens is not simply a function of porosity as stochastic materials such as open-celled metal foams and packed beds, but also a function of orientation (open area ratio). The overall heat transfer depends on porosity and surface area density, but only weakly on orientation. Comparisons with stochastic metal foams and other heat dissipation media such as packed beds, louvered fins and microtruss lattice cellular materials suggest that wire-screen meshes compete favorably with the best available heat dissipation media. The overall thermal efficiency index of the copper textiles-based media is approximately three times larger than that of stochastic copper foams, principally because of the lower pressure drop encountered during coolant propagation through the periodic wire-screen structure.

© 2004 Elsevier Ltd. All rights reserved.

**Keywords:** Forced convection; Cellular metals; Woven textiles; Louvered fins; Packed beds; Experiment; Thermal efficiency

### 1. Introduction

High porosity, ultra-lightweight, cellular metal structures with open cell topologies have emerged in the past decade as attractive heat exchange media for a wide range of applications where dissipation of high intensity heat over relatively small spaces is demanded [1,2]. These cellular metal structures can be classified into two broad classes, one with a stochastic topology (i.e. metal foams) and the other with a periodic structure [3–7]. A schematic illustration of several open and one closed celled periodic structure is shown in Fig. 1. Examples of the periodic structure include materials made from

stacked metal textiles and microtruss concepts with tetrahedral, pyramidal, Kagome and other types of topologies [3,4]. A wide variety of process-routes have been developed to manufacture cellular metals with relative densities of 1–20% and cell sizes from 100  $\mu\text{m}$  to several centimetres [5]. The open cell systems shown in Fig. 1(a)–(e) compare favourably with closed cell honeycombs (Fig. 1f) when used for the cores of sandwich panels [7]. They are therefore attracting considerable attention as multi-functional structures [7].

Several mechanisms contribute to heat transfer enhancements associated with the use of cellular metals, including interactions between the solid skeleton and a through-flowing fluid, and the importance of achieving a quality (low thermal resistance) metal-to-metal bond (brazing or transient liquid phase bonding is usually preferred over adhesive-bonding) [3]. Applications to

\* Corresponding author. Tel.: +44-1223-766316; fax: +44-1223-332662.

E-mail address: [tjl21@cam.ac.uk](mailto:tjl21@cam.ac.uk) (T.J. Lu).

**Nomenclature**

|            |  |                      |   |
|------------|--|----------------------|---|
| $A$        | heating area [m <sup>2</sup> ]                       | $q$                  | heat flux [W/m <sup>2</sup> ]                       |
| $B, B_0$   | empirical constants                                  | $R_{open}$           | open area ratio                                     |
| $C, C_0$   | empirical constants                                  | $Re_H$               | Reynolds number based on channel height             |
| $c_p$      | coolant specific heat                                | $t$                  | screen layer thickness                              |
| $d$        | wire diameter [m]                                    | $T_{f,bulk}$         | bulk mean temperature of coolant at inlet [K]       |
| $f$        | friction factor                                      | $T_w$                | temperature of bottom facesheet [K]                 |
| $H$        | height of testing sample [m]                         | $U_m$                | mean coolant velocity at inlet [m/s]                |
| $h$        | heat transfer coefficient [kW/m <sup>2</sup> K]      | $W$                  | width of testing sample [m]                         |
| $L$        | length of testing sample [m]                         | $w$                  | width of cell opening [m]                           |
| $l$        | total height of stacked layers [m]                   |                      |   |
| $K_f$      | coolant thermal conductivity [W/(m K)]               | <i>Greek symbols</i> |   |
| $n$        | total number of screen layers                        | $\alpha_{sf}$        | surface area density [1/m]                          |
| $N$        | number of pores per unit length, ( $N = 1/(w + d)$ ) | $\varepsilon$        | porosity  |
| $Nu_H$     | nusselt number based on channel height               | $\rho$               | density of copper made screens [kg/m <sup>3</sup> ] |
| $\Delta P$ | pressure drop [Pa]                                   | $\bar{\rho}$         | relative density                                    |
| $Q$        | input heat [W]                                       |                      |   |

53 electronics cooling and airborne multi-layer metal foam  
 54 heat exchangers have been investigated, revealing  
 55 promising advances in the rate of heat removal [6].  
 56 While commercial metal foams with open cells, which  
 57 are typical stochastic cellular structures, are good compact  
 58 heat exchangers and relatively cheap when made by  
 59 sintering, their load-bearing capability is much inferior  
 60 to periodic structures having the same weight. This  
 61 arises because their deformation under mechanical  
 62 loading is dominated by cell wall bending as opposed to  
 63 cell wall stretching in most periodic structures [7].  
 64 Nonetheless, as cross-flow heat exchangers they can  
 65 provide a high thermal conductivity path for heat

transport, a very high surface area for dissipation into a  
 cooling fluid located in the pores and a contiguous path  
 for forcing the coolant through the structure.  
 Topologically configured ultra-light metals with  
 periodic microtruss structures (tetrahedral, pyramidal,  
 Kagome etc.) have subsequently been developed (mainly  
 by rapid prototyping or injection molding, followed by  
 casting), which have good thermal, structural and other  
 performance characteristics [3,8]. A topological com-  
 parison between different microtruss structures is made  
 in Fig. 1. Their weight efficiency is as good as the best  
 competing concepts, with additional multi-functionality  
 advantages [8], but they are usually costly to manufac-

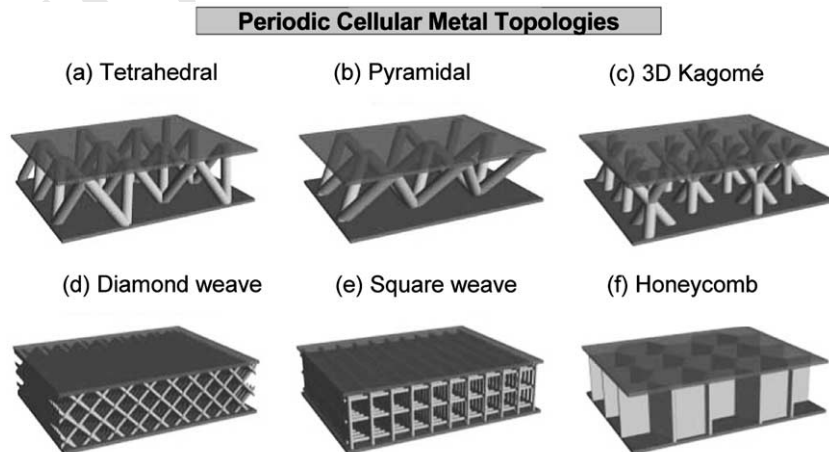


Fig. 1. Topological comparison of periodic structures.

79 ture. The use of a metal textile technology coupled with  
80 novel bonding strategies to create periodic, cellular  
81 structures has the potential to improve the performance/  
82 cost ratio [3].

83 The metal textile derived cellular metals are the three-  
84 dimensional analogue of metallic textile screen meshes  
85 which have already been extensively used in fields such  
86 as aerospace, chemical product, food processing, air  
87 conditioning/refrigeration, and medicine [8]. Analytical  
88 models, backed with experimental measurements, have  
89 been developed to characterize the porosity, flow resis-  
90 tance, and heat transfer of wire-screen meshes [9–15].  
91 Due to anisotropy, the thermal characteristics are ori-  
92 entation dependent, which cause different overall heat  
93 transfer in different directions, and hence lead to opti-  
94 mization opportunities. To meet the need for the design  
95 of heat pipes and Stirling engine regenerators, a number  
96 of studies have focused on predicting the effective ther-  
97 mal conductivity of fluid-saturated wire screens [10,11].  
98 Duprat and Lopez [12] compared the thermal perfor-  
99 mance of three different heat regenerator media:  
100 monolith, stack of woven screens and a packed bed of  
101 spheres. Based on a given heat transfer efficiency, the  
102 energy efficiency of stacked wire screens was found to  
103 cover a wider range of gauges. Ahmad et al. [15] studied  
104 the thermo-physical characteristics of various heat  
105 transfer media, and found that copper woven screens are  
106 promising thermal energy absorber matrices for packed-  
107 bed solar air heaters. Hsu et al. [16] developed an ana-  
108 lytical model for the effective stagnant thermal conduc-  
109 tivity of wire screens.

110 As far as heat transfer in woven-screen meshes is  
111 concerned, previous studies have mainly focused on a  
112 single screen layer or self-supporting layers of screens  
113 stacked together without bonding. Jiang et al. [17] car-  
114 ried out a combined experimental and numerical study  
115 on forced convective heat transfer in packed beds of  
116 sintered and non-sintered copper spheres, and found  
117 that, due to reduced thermal contact resistance, sintering  
118 can increase the overall heat transfer to a cross-flowing  
119 fluid. The increases can be large: up to 15 times for water  
120 and 30 times for air. We note that such bonding also  
121 dramatically modifies the mechanical properties and  
122 creates opportunities for multi-functional applications  
123 of the type recently envisioned [1,7]. In this study,  
124 sandwich panels with woven-screen cores having dia-  
125 mond or square-shaped pores are fabricated by using the  
126 TLP bonding and brazing methods to create robust  
127 nodes at wire crossovers and between the laminae. The  
128 overall heat transfer performance of the panels under  
129 forced air convection is measured along different orien-  
130 tations, and is compared with metal foams, microtruss  
131 materials, packed beds, louvered fins and other heat  
132 dissipation media is made.

## 2. Test samples 133

### 2.1. Fabrication of TLP bonded and brazed textile heat 134 sink 135

The potentially inexpensive textile-based approach 136  
for the synthesis of wire-screen laminates is illustrated in 137  
Fig. 2. Prototype sandwich heat sinks with laminated 138  
textile cores of plain woven copper cloth (obtained from 139  
GDC/City Wire Cloth Co., Fontana, CA) were fabri- 140  
cated using two similar methods: transient liquid phase 141  
(TLP) bonding and brazing. The wire alloy was C110000 142  
copper (99.95Cu–0.04O) with a density of  $\rho_s = 8.89 \text{ g/}$  143  
 $\text{cm}^3$  and a thermal conductivity of  $k_s \approx 385 \text{ W/(mK)}$  at 144  
ambient conditions. 145

For TLP bonding operation, laminae were first 146  
lightly sprayed with a mix of polymer-based cement 147  
(Nicrobraz<sup>®</sup> Cement 520) and Ni–25Cr–10P braze alloy 148  
powder (Nicrobraz<sup>®</sup> 51), both supplied by Wal 149  
Colmonoy Corp. (Madison Heights, MI). The solidus 150  
and liquidus of this alloy are 880 and 950 °C whereas the 151  
melting point of copper is 1083 °C. The coated laminae 152  
were then heated within flowing argon (at a vacuum 153  
level of approximately  $10^{-1}$  Torr), at a rate of 20 °C/min 154  
to 550 °C to volatilize the polymer cement. An impor- 155  
tant feature of this braze/cement combination is that the 156  
braze alloy powders adhered to the wires after volatiliza- 157  
tion. The system was then evacuated to a vacuum level 158  
of less than  $10^{-3}$  Torr and the temperature was ramped 159  
at a rate of 20 °C/min to 1000 °C and held there for 15  
min. During this final heating, the braze alloy powders 161  
melted, coated the wires (this seals microscopic defects, 162  
if any), and the melt was preferentially drawn by capil- 163  
lary action to points of wire contact. This initial node 164  
rigidization procedure helps with more accurate stacking 165  
and alignment of multiple plies upon laminating. The 166  
rigidized laminae were again sprayed with the cement/ 167  
powder mix and then stacked peak to peak (using pins 168  
to align all openings). A small compressive pressure was 169  
applied to the periphery of the lay ups and the volatili- 170  
zation/heating procedure was repeated to construct the 171  
multi-laminate cores (Fig. 2a). To construct a sandwich, 172  
0.813 mm thick facesheets were sprayed and the vola- 173  
tilization/heating procedure was applied to metallurgi- 174  
cally bond them to the textile cores (Fig. 2b). The solid 175  
facesheets are made of the same alloy as the wires. 176

For the brazing operation, individual laminae were 177  
stacked, with alignment achieved using threaded guide 178  
pins to align all openings. The laminae were stacked 179  
peak to peak to ensure a regular structure. A small 180  
compressive pressure was then applied to the guide pins 181  
to maintain contact at the peak to peak nodes. The 182  
entire assembly was then dipped into a viscous brazing 183  
paste of CuproBraz<sup>®</sup>. The CuproBraz<sup>®</sup> process is a 184  
brazing process specifically developed for the manufac- 185

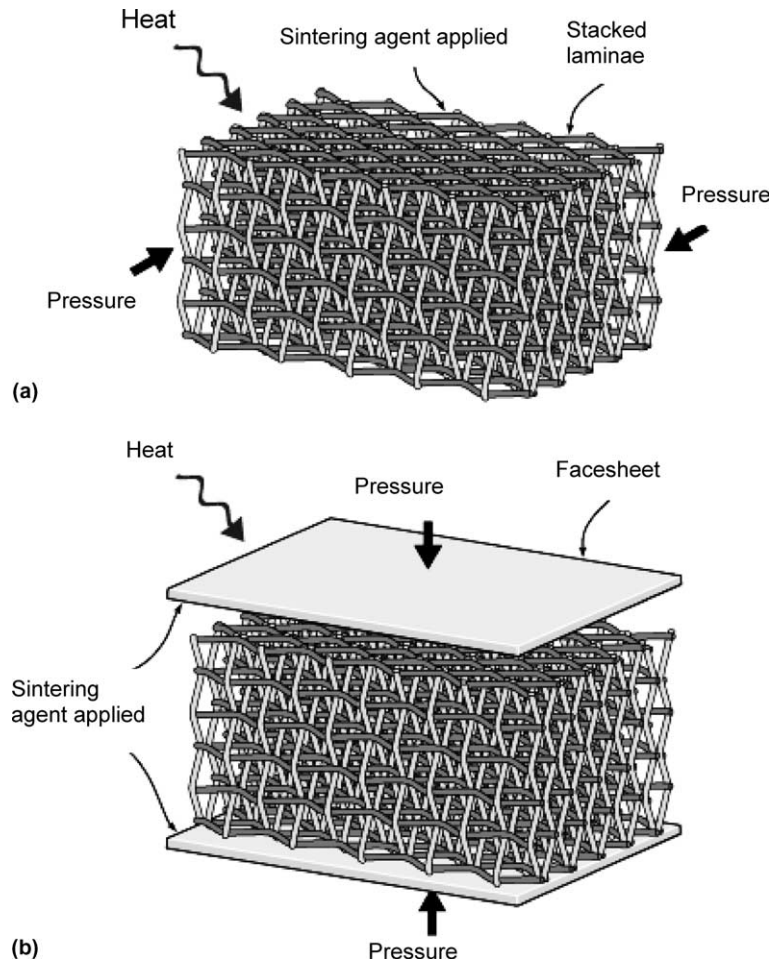


Fig. 2. Sandwich construction with textile technology: (a) a transient liquid phase joins the wire-mesh screen laminated at all points of contact; (b) facesheets are added to the textile core.

186 turing of automotive and heavy-duty industrial heat  
187 exchangers. By using high strength and high conductivity  
188 copper and copper alloys it is possible to manufacture  
189 light, strong, efficient and compact heat exchangers  
190 at a low cost with this environmentally friendly process.  
191 The brazing filler metal, developed for CuproBraz<sup>®</sup>,  
192 belongs to the CuSnNiP-family. This filler metal is  
193 called OKC600 and has a nominal composition of:  
194 Ni-42%, Sn-15.6%, P-5.3%, Cu-balance. The braze  
195 coated assemblies were air dried in a warming oven  
196 then transferred to a vacuum furnace and heated  
197 under a partial pressure of argon (250 mTorr) at a  
198 rate of 30 °C/min to 650 °C and held for 15 min,  
199 followed by a rapid furnace cool. Finally, the  
200 brazed core assemblies were machined to size and  
201 solid copper facesheets were attached using the same  
202 brazing process.

202 The sandwich panels thus created can be designed to  
203 carry structural load at minimum weight, while simul-

204 taneously allowing fluid passage for cooling or other  
205 purposes.

## 2.2. Topology of textile core 206

207 Fig. 3 shows the typical topology of the samples  
208 tested; the detail of each test sample is listed in Table 1,  
209 where samples made with square-shaped screens are  
210 designated S and those with diamond-shaped screens as  
211 D. When viewed perpendicular to the mesh, the structure  
212 had square or diamond openings with a relative large  
213 open area for fluid passage. When viewed from the  
214 side, the individual layers formed a triangular pattern  
215 with significantly less open fluid passage. The sample  
216 sides were machined mutually orthogonal. Samples S-1  
217 and S-2 have identical cores, except for their orientation  
218 relative to the facesheet. For sample S-1, the trusses  
219 are all parallel to the facesheets, such that the passage  
220 of fluid flow is through the stagger-shaped pores between

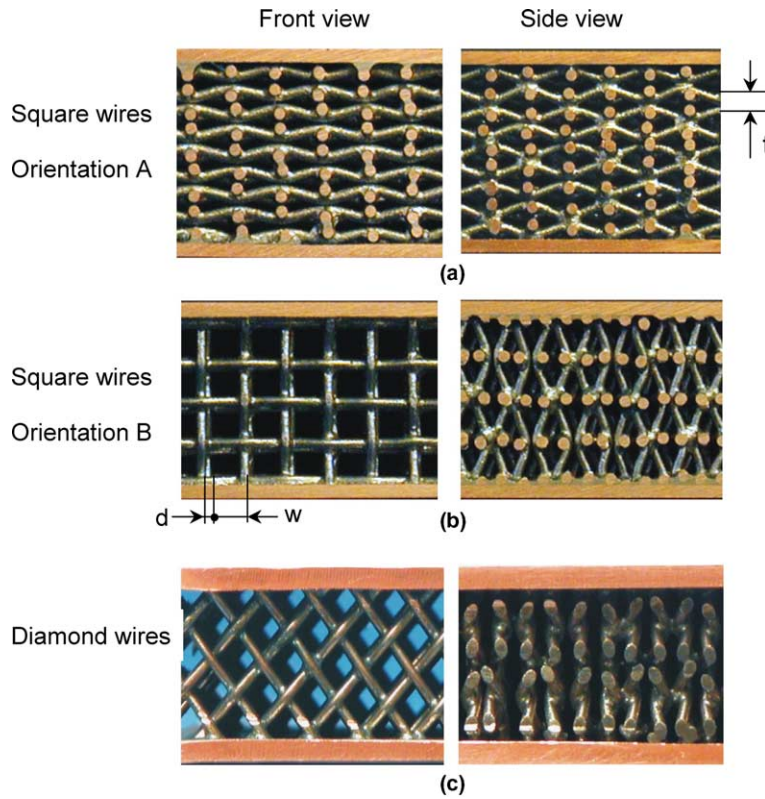


Fig. 3. Textile laminate heat exchangers: (a) images of orientation A with square-shaped pores; (b) images of orientation B with square-shaped pores; (c) images of diamond-shaped pores.

Table 1  
Morphological parameters for all brazed wire-screen samples

| Sample number        | Material make | Wire diameter (mm) | Aperture (mm) | Porosity | Surface area density (m <sup>2</sup> /m <sup>3</sup> ) |
|----------------------|---------------|--------------------|---------------|----------|--|
| <i>Square shape</i>  |               |                    |               |          |  |
| Orientation A        |               |                    |               |          |  |
| S-1                  | Pure copper   | 0.635              | 1.905         | 0.798    | 1237   |
| Orientation B        |               |                    |               |          |  |
| S-2                  |               | 0.635              | 1.905         | 0.798    | 1237   |
| S-3                  |               | 0.8                | 1.300         | 0.680    | 1496   |
| S-4                  |               | 0.9                | 2.800         | 0.803    | 849  |
| <i>Diamond shape</i> |               |                    |               |          |  |
| D-1                  | Pure copper   | 0.8                | 2.360         | 0.795    | 994  |
| D-2                  |               | 1.0                | 2.130         | 0.737    | 1004   |
| D-3                  |               | 1.2                | 1.980         | 0.683    | 988  |
| D-4                  |               | 0.8                | 1.300         | 0.680    | 1496   |

221 stacked laminate (see Fig. 3a). For samples S-2 to S-4,  
222 the trusses are parallel and perpendicular to the face-  
223 sheets, with flow directed along the aligned square pores  
224 (see Fig. 3b). For samples D-1 to D-4, the trussed are  
225 oriented 45 degree to the facesheets, with flow directed  
226 along the aligned diamond pores (see Fig. 3c). All  
227 samples have width  $W = 40$  mm (same as the width of

the testing channel), core height  $H = 10$  mm, facesheet  
thickness  $0.813$  mm, and length  $L = 60$  mm. 228 229

### 2.3. Porosity and surface area density 230

The woven screens have a wire diameter  $d$ , width of  
square pore  $w$ , and screen layer thickness  $t = 2d$  (Fig. 3). 231 232

233 The number of pores per unit length,  $N$  (mesh number),  
234 is

$$N = \frac{1}{d + w} \quad (1)$$

236 For the present samples,  $N$  takes the value of 8, 10 and  
237 12 pores/in. With  $\rho$  denoting the density of the screens,  
238 the relative density of a brazed mesh screen laminate can  
239 be calculated as [10]

$$\bar{\rho} \equiv \frac{\rho}{\rho_s} = \frac{\pi N d^2}{2(l/n)} \sqrt{1 + \left(\frac{1}{1 + w/d}\right)^2} \quad (2)$$

241 where  $\rho_s$  is the solid material density,  $n$  is the total  
242 number of stacked layers of height  $l$ , and the effect of  
243 bonding has been neglected. As an individual layer is in  
244 a bed which can be either compacted or distended, its  
245 volume is determined by  $l/n$  instead of the wire diameter  
246  $t$ . The square-root term in (2) is introduced to account  
247 for the effect of crimping of wires during weaving. It has  
248 a value less than 1.03 when  $w/d > 3$ . The measured  
249 value of  $\bar{\rho}$  is slightly smaller (around 1%) than the value  
250 predicted by (2), due to the added weight of bonding  
251 agent at contact points.

252 The porosity  $\varepsilon$  of the laminate core is related to  $\bar{\rho}$  by  
 $\varepsilon = 1 - \bar{\rho}$  (3)

254 Another mesh parameter important for subsequent  
255 heat transfer analysis is the surface area density  $\alpha_{sf}$  (total  
256 surface area per unit volume), given by

$$\alpha_{sf} = \frac{\text{total surface area}}{\text{volume}} = \frac{\pi}{w + d} = \pi N \quad (4)$$

258 A large surface area density is desirable for enhanced  
259 thermal transport in a compact heat exchanger. The  
260 surface area density is governed by the number of pores  
261 per unit length,  $N$ . From Eqs. (2) and (4),  $\alpha_{sf}$  increases as  
262 the relative density is increased for a given wire diameter.  
263 With the relative density fixed,  $\alpha_{sf}$  decreases as the  
264 wire diameter is increased. The value of  $\alpha_{sf}$  can be  
265 engineered to exceed 2000 m<sup>2</sup>/m<sup>3</sup> when  $N > 18$  pores/in.  
266 This is comparable to the corresponding value of com-  
267 mercially available metal foams having similar pore sizes.  
268 It is significant larger than that of pin fin arrays and  
269 microtruss materials having the same relative density,  
270 making wire screens potentially attractive as compact  
271 heat exchangers.

### 272 3. Experiments

#### 273 3.1. Test set-up and data acquisition procedures

274 A schematic diagram of the test rig for pressure drop  
275 and heat transfer measurements is shown in Fig. 4a. The  
276 main components are: air supply, test section, heating

arrangement, and data acquisition. An open-circuit  
suction-type wind tunnel was constructed for this study.  
Ambient air, as coolant, is drawn into a rectangular  
Perspex channel (0.025 m width and 0.01 m height)  
containing the test section. Before reaching the test  
section, efforts were made to ensure the coolant flow was  
fully developed. To achieve this, the coolant first flows  
through a wire-screen layer (wire diameter = 0.56 mm),  
followed by a 4:1 contraction section, a honeycomb  
layer, another wire-screen layer, and a relatively long  
parallel plate channel (with a ratio of section length to  
channel height,  $L1/H = 35$ ).

A stagnation pressure tapping was placed at the  
centre and adjacent wall static pressure tapping was used  
for mid-height flow velocity measurement. Given that  
the ratio of channel height (10 mm) to outer diameter  
(0.51 mm) of the tube is 19.6, the wall interference on the  
pressure tapings is expected to be negligible. The inlet  
coolant velocity profile along the channel height was  
measured to calculate the mean flow velocity. For  
pressure drop measurements, two static pressure tap-  
pings monitored by a digital manometer were positioned  
at the inlet and outlet of the test section, respectively.

Fig. 4b shows the typical inlet coolant velocity profile  
over the channel height. When the velocity at the mid-  
height  $U_c$  is smaller than 2.7 m/s, the flow is developing;  
the flow is fully developed when  $U_c$  exceeds this value.  
The mean velocity  $U_m$  is correlated with  $U_c$  as

$$U_m = 0.84U_c - 0.26 \quad (5)$$

For heat transfer measurement, an isoflux (constant  
wall heat flux) boundary condition was imposed on the  
bottom facesheet of the test sandwich by a heating pad  
(silicone-rubber etched foil from Watlow™ Inc.), whilst  
the top facesheet is thermally insulated. A pure copper  
heat spreader plate, 0.9 mm thick, was inserted between  
the heating element and the bottom facesheet to ensure  
the uniformity of the heat flux. Four thin (0.013 mm  
thickness) T-type copper-constantan foil thermocouples  
(butt bonded) were mounted onto the bottom facesheet  
along the centreline in the flow direction. Two additional  
T-type bead thermocouples were positioned separately  
at the inlet and outlet of the test section to measure the  
coolant temperature at mid-height at each location. All  
measurements were performed under steady-state con-  
ditions and repeated until significant data repetition was  
ensured, i.e., 5% uncertainty interval (see measurement  
uncertainties discussed below). The test conditions are  
listed in Table 1.

#### 3.2. Data reduction parameters

Experimentally, Kim et al. [18] observed that in an  
open-celled metal foam with stochastic but otherwise  
homogeneous cellular structure, fluid-flow pattern re-

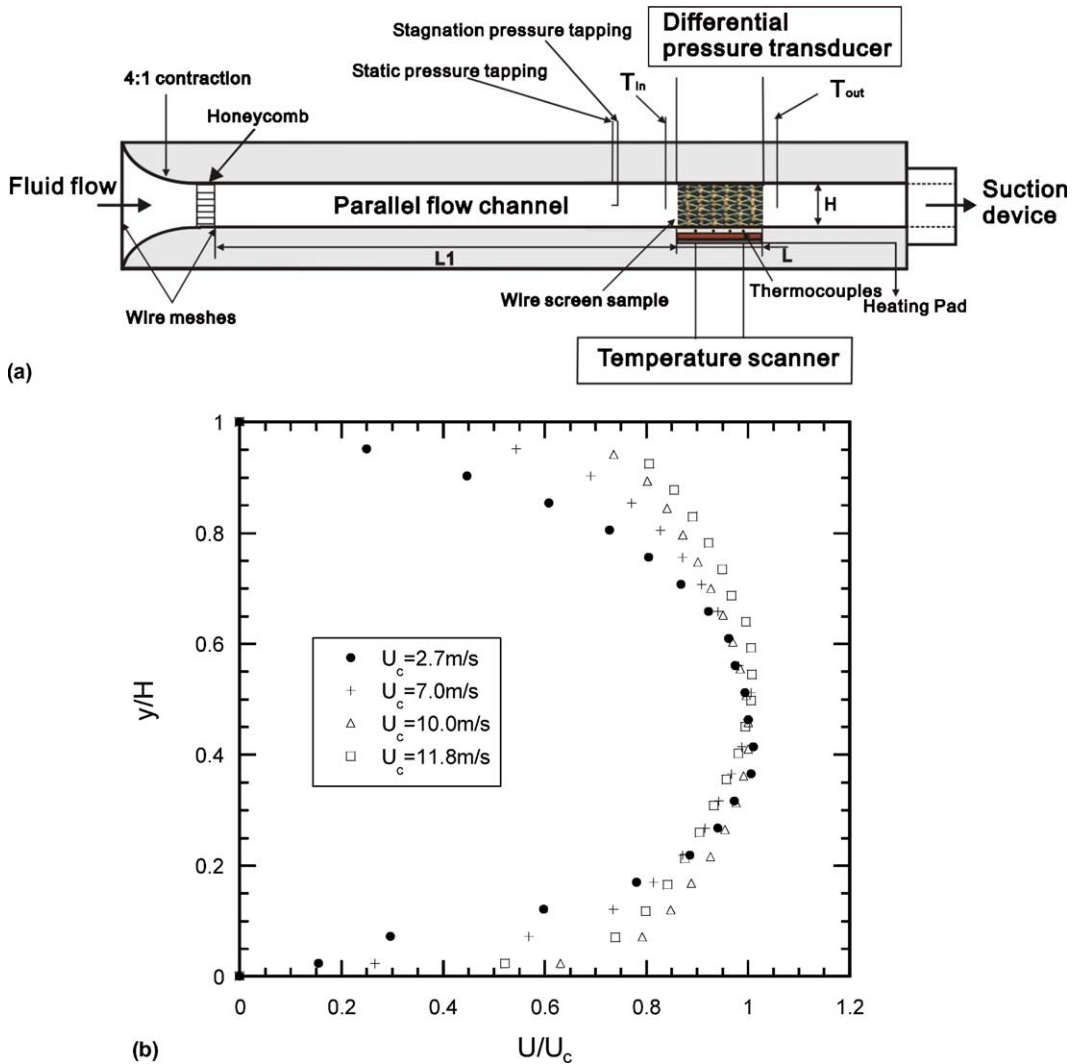


Fig. 4. Experimental set-up: (a) forced air convection test rig; (b) measured inlet flow velocity profile along the channel height.

329 peats over blocks of foam cells (excluding those near the  
 330 entrance and exit regions). Information obtained from a  
 331 representative unit cell can therefore be utilized to de-  
 332 scribe the whole structure. The pressure loss coefficient  
 333 and Nusselt number defined on the basis of a unit cell  
 334 have been successfully used by Kim et al. [18] to corre-  
 335 late a multitude of test data from metal foams with  
 336 different morphological features (pore size, porosity,  
 337 etc.). In this paper, we use channel height  $H$  as the length  
 338 scale, in order to compare the test data obtained for wire  
 339 screens with those of traditional heat dissipation media.  
 340 Reynolds number and friction factor based on the  
 341 channel height are defined as

$$Re_H = \frac{\rho_f U_m H}{\mu_f} \quad (6)$$

$$f = \left( \frac{\Delta P}{L} \cdot H \right) \cdot \left( \frac{1}{\rho U_m^2 / 2} \right) \quad (7)$$

344 where  $U_m$  is the mean coolant velocity at the inlet of the  
 345 test section,  $\rho_f$  and  $\mu_f$  are the coolant density and vis-  
 346 cosity, and  $\Delta P/L$  is the pressure drop per unit length.  
 347 For all the samples tested, the mean inlet coolant  
 348 velocity varies from 1.0 to 10 m/s (see Fig. 4b). The  
 349 lower bound of coolant velocity was set by the stability  
 350 of flow whilst the upper bound was limited by pumping  
 351 capacity.

352 For heat transfer characterization, the heat transfer  
 353 coefficient  $h$  and the corresponding Nusselt number  $Nu_H$   
 354 are defined as

$$h = \frac{Q}{A} \frac{1}{\Delta T} = \frac{q}{T_w - T_{f,bulk}} \quad (8)$$

$$Nu_H = \frac{h \cdot H}{k_f} \quad (9)$$

357 where the coordinate  $x$  measures from the entrance of  
 358 the testing sample in the main flow direction,  $k_f$  is the  
 359 thermal conductivity of the coolant, and  $q = Q/A$  is the  
 360 input heat flux. Here,  $Q$  is the input rate of heat,  $A$  is the  
 361 heating area (namely, the copper substrate area),  $T_w$  is  
 362 the temperature of the bottom facesheet, and  $T_{f,bulk}$  is  
 363 the bulk mean temperature of the coolant at inlet.

### 364 3.3. Measurement uncertainty

365 An uncertainty analysis was performed by using the  
 366 method described in Coleman and Steele [19]. The  
 367 maximum heat loss through insulation materials was  
 368 estimated to be less than 2% of the total input heat. The  
 369 variation in the thermal conductivity of air,  $k_f$ , is neg-  
 370 ligible in the operating temperature range of 300–330 K,  
 371 whereas its density varies by about 5%. The uncertainty  
 372 in pressure drop measurement was estimated to be less  
 373 than 5%. The uncertainties calculated from the root-  
 374 square method for the mean heat transfer coefficient,  
 375 Reynolds number and Nusselt number were estimated to  
 376 be less than 5.3%, 5.7% and 5.4%, respectively.

## 377 4. Pressure loss

378 Ideally, a compact heat exchanger should have a high  
 379 rate of heat transfer with a low pressure drop. The  
 380 brazed wire screens are structurally periodic and deter-  
 381 ministic but orthotropic. Friction factors of all the test  
 382 samples are plotted in Fig. 5. Samples tested in different  
 383 orientations, with different pore shapes and different  
 384 porosities, show different ranges of friction factors. The  
 385 relevant parameters of all the samples are summarized in  
 386 Table 2.

### 387 4.1. Effect of flow orientation

388 As described in Section 2.2 and seen in Fig. 3, ori-  
 389 entation A of a sample has completely different flow  
 390 passages in comparison with orientation B. The flow  
 391 passages in the former are staggered, whilst in the latter  
 392 the flow passages are more open and the pores are  
 393 square (or diamond) shaped. Therefore, it would be  
 394 interesting to compare the thermal and hydraulic of  
 395 samples S-1 and S-2 having identical wire diameter  
 396 (0.635 mm), pore shape (square), aperture (1.905 mm)  
 397 and porosity ( $\varepsilon = 0.795$ ), but different orientations.

398 When  $Re_H < 1000$  for S-1 or  $Re_H < 1500$  for S-2, the  
 399 flow is dominated by viscosity (Fig. 5), with the friction

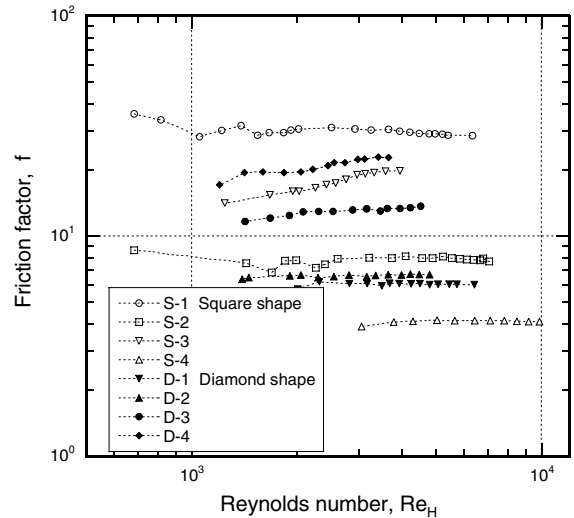


Fig. 5. Friction factor plotted as a function of Reynolds number based on channel height for brazed textiles.

Table 2  
Experimental operating conditions

| Parameters             | Ranges        |
|------------------------|---------------|
| Inlet coolant velocity | 1.0–10 m/s    |
| Reynolds number $Re_H$ | 700–10000     |
| Inlet temperature      | 290.0 K       |
| Outlet temperature     | 300.0–320.0 K |

factor decreasing with increasing  $Re_H$ . At higher Rey-  
 400 nolds numbers, the friction factor is nearly constant, as  
 401 the flow is form dominated. At a given Reynolds num-  
 402 ber in the form-dominant regime, it is seen from Fig. 5  
 403 that the friction factor of S-1 (orientation A) is about  
 404 three times larger than that of S-2 (orientation B),  
 405 implying that the resistance encountered by the flow in  
 406 orientation A is much higher than that in orientation B.  
 407 For isotropic stochastic materials such as foams and  
 408 packed beds, friction factor in the high Reynolds num-  
 409 ber regime is mainly a function of porosity.  
 410

Because wire screens are intrinsically anisotropic,  
 411 flow passages are different along different orientations,  
 412 even though the porosity remains unchanged. Therefore,  
 413 parameters in addition to the porosity must be intro-  
 414 duced. In order to quantify the contribution of blockage  
 415 effect on pressure drop, the open area ratio of a sample is  
 416 defined as  
 417

$$R_{open} = \frac{\text{Open area}}{\text{Total area}} \quad (10)$$

where open area is the void area in the front view, and  
 419 total area is the whole area in the front view. The open  
 420 area ratio (0.25) of sample S-1 is approximately half that  
 421

422 of sample S-2 (0.56). Consequently, the measured pres-  
423 sure drop across S-2 is significantly lower than that  
424 across S-1, implying that the pressure loss in the current  
425 range of fluid flow is mainly attributable to the difference  
426 in form drag across the wire screens. In general, friction  
427 factor increases as the open area ratio is decreased.

428 4.2. Effect of pore shape

429 Samples S-3 and D-4 have identical wire diameter,  
430 aperture and porosity, but different pore shapes (square  
431 versus diamond, see Fig. 3b and c). The friction factor of  
432 D-4 is slightly higher than that of S-3, attributable  
433 mainly to the cells near top and bottom substrates of the  
434 sandwich. Due to machining, these cells are only half or  
435 even smaller of a whole unit cell, and hence have dif-

436 ferent flow patterns in comparison with those in the core  
437 centre. However, at high Reynolds numbers, the flow  
438 drag behind each wire ligament is the main reason for  
439 the overall pressure loss through a wire-screen structure:  
440 the contribution caused by the boundary layer near the  
441 top and bottom substrates is relatively small.

442 4.3. Effect of porosity and open area ratio

443 Fig. 6a and b plot separately the friction factor  $f$  as a  
444 function of open area ratio  $R_{open}$  and porosity  $\epsilon$  at  
445  $Re_H = 4000$ . Note that the flow resistance decreases with  
446 increasing  $R_{open}$  and increasing  $\epsilon$ . Except for sample S-1  
447 (orientation A), Fig. 6a and b exhibit similar trends,  
448 suggesting that square shape and diamond shape sam-  
449 ples have similar flow patterns. When the flow channel

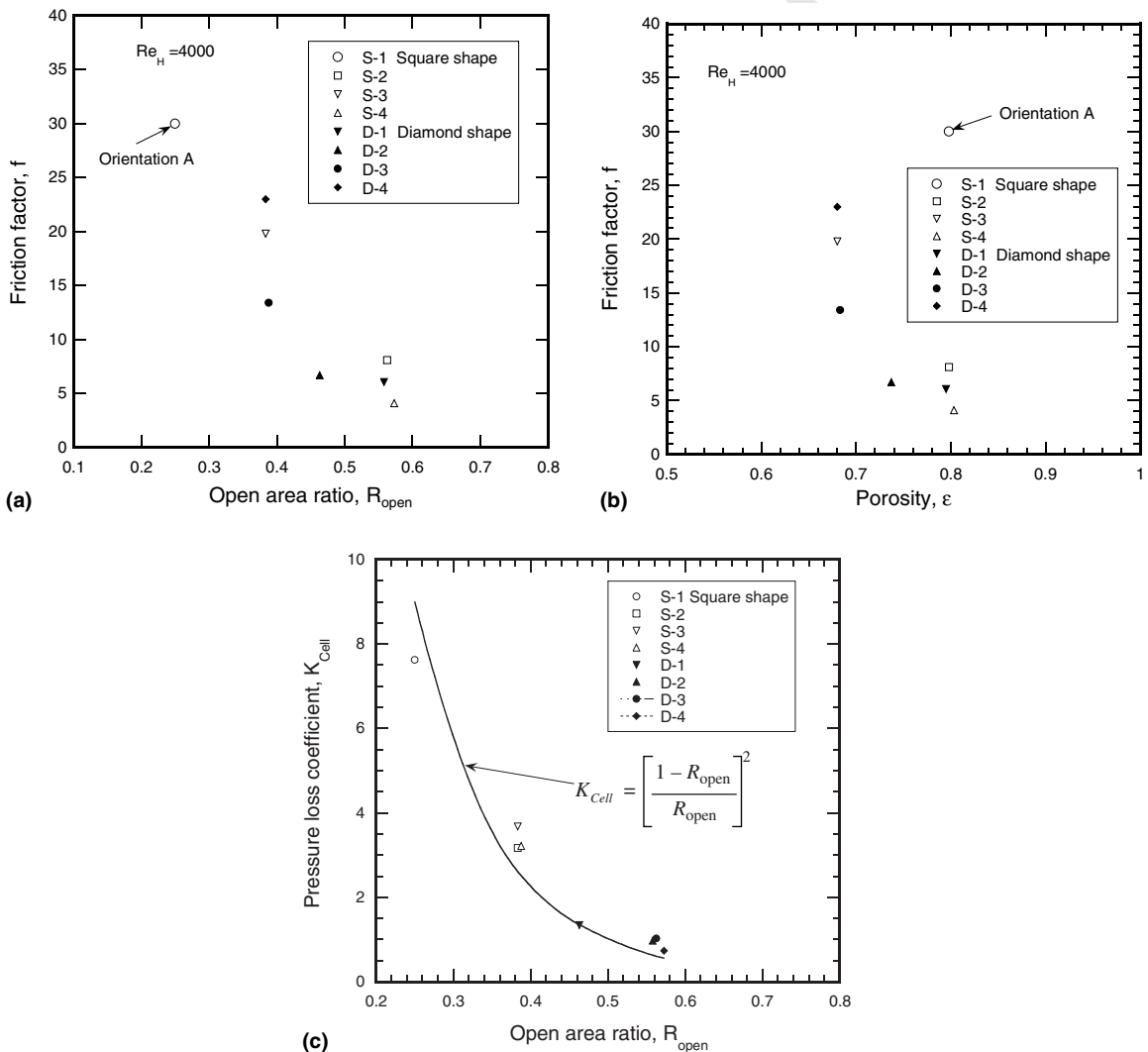


Fig. 6. Effect of (a) porosity and (b) open area ratio on friction factor of woven textiles at  $Re_H = 4000$ ; (c) pressure loss coefficient  $k_{cell}$  plotted as a function of open area ratio at  $Re_H = 4000$ .

450 width is much larger than the channel height, the flow  
451 resistance mainly depends on flow mixing, with negli-  
452 gible contribution from the partial cells near the substrate  
453 walls. Because the open area ratio and porosity are both  
454 functions of the ratio of wire diameter to aperture,  $d/w$ ,  
455 porosity can be expressed in terms of open area ratio  
456 and vice versa. However, the results of Fig. 6a and b  
457 suggest that  $R_{\text{open}}$  or  $\varepsilon$ , both non-dimensional, cannot be  
458 used to uniquely characterize the flow resistance of a  
459 wire-screen structure: other parameters need to be  
460 introduced.

461 Due to geometrical similarity, the principle of flow  
462 passing through an orifice plate may be used to describe  
463 pressure loss across a wire screen. The basic mathe-  
464 matical derivations using continuity and momentum  
465 equations are given in the Appendix A, leading to a new  
466 definition of friction factor (pressure loss coefficient)  
467  $K_{\text{Cell}}$  based on unit cell length  $d_p$  as

$$K_{\text{Cell}} = \frac{\Delta P_{\text{Cell}}}{\rho U_m^2 / 2} = \left( \frac{\Delta P}{L} \cdot d_p \right) \cdot \left( \frac{1}{\rho U_m^2 / 2} \right) \\ = \left( \frac{1 - R_{\text{open}}}{R_{\text{open}}} \right)^2 \quad (11)$$

469 where, for orientation A,  $d_p = d + w$ , and for orientation  
470 B,  $d_p = 2d$ . The comparison between the master curve  
471 predicted from (11) and experimental data is shown in  
472 Fig. 6c for all the samples tested, with reasonably good  
473 agreement observed. In other words, the pressure loss  
474 across a unit cell can be described by a single parameter  
475  $R_{\text{open}}$  (or  $\varepsilon$ ). The same conclusion has been reached for  
476 stochastic metal foams [18].

## 477 5. Heat transfer performance

478 The heat transfer performance of all the copper  
479 structures is compared in Fig. 7, where both the Nusselt  
480 number and Reynolds number are based on the channel  
481 height. Note that the porosity of wire screens tested in  
482 this study ranges from 0.68 to 0.8, significantly smaller  
483 than that of metal foam ( $>0.9$ ) [1,6] but much larger  
484 than that of packed beds [2]. Conduction through solid  
485 ligaments is therefore more important in brazed wire  
486 screens than that in metal foams (as well as that in  
487 packed beds without brazing), especially with high  
488 thermal conductivity materials (pure copper in current  
489 study). The overall heat transfer includes forced con-  
490 vention through wire screens, conduction through sub-  
491 strates as well as wire screens.

### 492 5.1. Effect of flow orientation

493 At a given Reynolds number, Sample S-2 has a larger  
494 Nusselt number than that of S-1 (Fig. 7), even though its  
495 flow resistance is much smaller than the latter (Fig. 5).

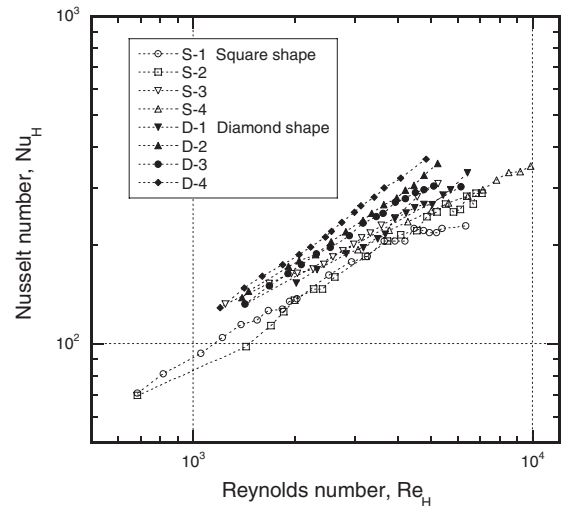


Fig. 7. Nusselt number plotted as a function of Reynolds number based on channel height for woven textiles.

496 Also, the heat transfer rate of S-2 increases slightly faster  
497 than S-1 as the Reynolds number is increased (Fig. 7). 497

498 As can be seen from Fig. 3, S-2 has a continuous  
499 solid path along the channel height, whilst S-1 has  
500 brazed joints between stacked layers. The material be-  
501 tween joints is nickel, with a thermal conductivity much  
502 smaller than pure copper. It is expected therefore that S-2  
503 has a larger effective thermal conductivity along the  
504 channel height than that of S-1. This is important be-  
505 cause, during the experiment, heat is supplied from the  
506 bottom facesheet while fluid flows in a direction per-  
507 pendicular to the direction of heat.

508 Another likely reason for the superior performance  
509 of S-2 to S-1 lies in the different flow patterns in these  
510 two samples. From the well established study of bank of  
511 cylinders, it is known that the flow pattern behind one  
512 cylinder depends on the arrangement of cylinders. If the  
513 distance of two rows of cylinder is too close, the vortex  
514 after the first row is yet to complete when the new vortex  
515 starts; on the other hand, if the distance is sufficiently  
516 large for vortices to complete, the flow is less turbulent.  
517 From the heat transfer point of view, the flow pattern  
518 developed in S-1 is not as efficient as that in S-2,  
519 even though the flow encounters much higher resistance  
520 in S-1.

### 521 5.2. Effect of pore shape

522 Samples S-3 and D-4 are identical, except that the  
523 pores in the former are square and those in the latter are  
524 diamond. Because both samples have approximately the  
525 same flow resistance (Fig. 5) and flow pattern (excluding  
526 regions near the substrates), it is expected that the con-  
527 tribution of forced convection on the overall heat

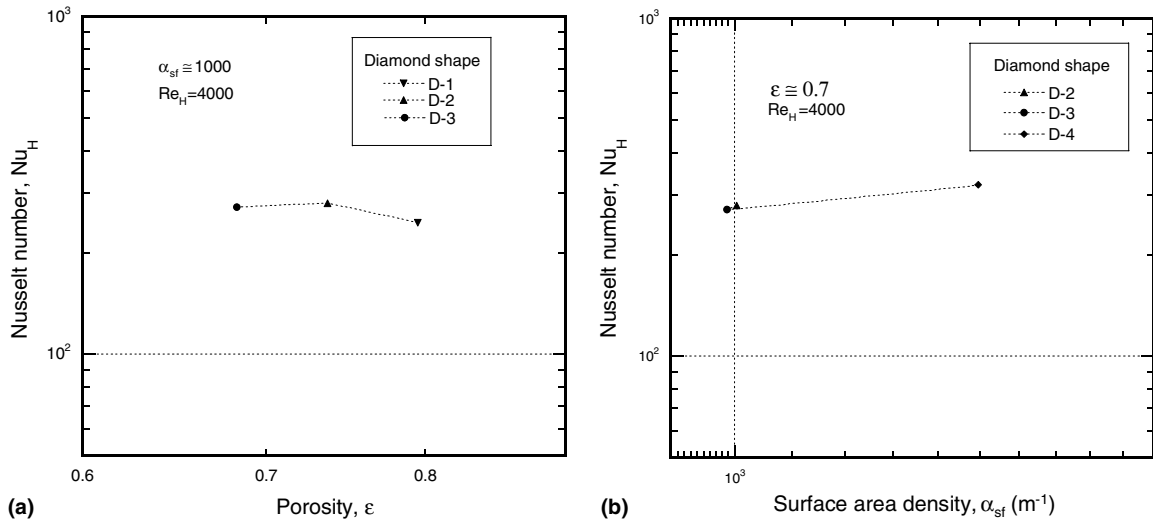


Fig. 8. Effect of (a) porosity with fixed surface area density and (b) surface area density with fixed porosity on Nusselt number at  $Re_H = 4000$ .

528 transfer is nearly the same for these two samples.  
 529 However, the experimental data in Fig. 7 reveal that  
 530 the Nusselt number of D-4 is 20–30% higher than that of  
 531 S-3. The difference is mainly attributable to the different  
 532 contribution from conduction through wire ligaments.  
 533 From Fig. 3, it can be seen that the solid wire elements in  
 534 a diamond shape sample (D-4) have approximately 40%  
 535 more contact area with the substrates than those in a  
 536 square shape sample (S-3), leading to a higher effective  
 537 thermal conductivity in the direction of channel height.  
 538 If the two samples are made with a low conductivity  
 539 material (e.g., polymer), they would have the same heat  
 540 dissipation capability because the contribution from  
 541 solid conduction is negligible in comparison with that  
 542 due to convection. This has been verified experimentally  
 543 by Kim et al. [20] for lattice-frame materials.

### 544 5.3. Effect of porosity and surface area density

545 Surface area density represents the total surface area  
 546 per unit volume, whereas porosity represents the per-  
 547 centage of void per unit volume. Because pure copper  
 548 has a high thermal conductivity, the contribution of  
 549 thermal conduction through wire ligaments cannot be  
 550 ignored. Consequently, both the surface area density  
 551 and porosity are important characteristics for copper  
 552 wire meshes. In the following discussion, one of the two  
 553 parameters is fixed while the other is varied in order to  
 554 isolate the effects.

555 Fig. 8a plots the Nusselt number of samples D-1, D-2  
 556 and D-3 as a function of porosity; the surface area  
 557 density of the three samples with diamond-shaped pores  
 558 is approximately  $1000 \text{ m}^{-1}$  and Reynolds number is

559 fixed at 4000. The overall heat transfer rate appears to  
 560 decrease if the porosity is increased beyond 0.75 or de-  
 561 creased below 0.70. Higher porosity means less solid  
 562 material per unit volume, and hence less conduction  
 563 through wire ligaments. Lower porosity means less void  
 564 volume per unit volume, and hence less contribution of  
 565 forced convection. It is likely therefore that there exists  
 566 an optimal porosity for maximum heat transfer at a  
 567 given surface area density. For the samples tested here,  
 568 this porosity lies in the range between 0.7 and 0.75.  
 569 More experiments, complemented with theoretical  
 570 modelling, will be conducted in a future study to further  
 571 highlight this important feature of cellular structures  
 572 made with a high conductivity material.

573 Fig. 8b illustrates the effect of surface area density on  
 574 the heat transfer capability of samples D-2, D-3 and D-4  
 575 at a fixed porosity level ( $\epsilon \cong 0.7$ ) and a given Reynolds  
 576 number ( $Re_H = 4000$ ). At a given porosity, the amount  
 577 of heat dissipated increases with increasing surface area  
 578 density. A higher surface area density corresponds to a  
 579 larger surface area per unit volume between fluid and  
 580 solid, and hence more heat can be transferred by the  
 581 fluid.

## 582 6. Comparison of heat dissipation media

583 The following different types of porous heat dissipa-  
 584 tion medium listed in Table 3 are compared: brazed  
 585 copper textiles (excluding S-1 with orientation A), lat-  
 586 tice-frame materials (LFMs, aluminum alloy) [20,21],  
 587 Kagome structures (bronze) [22], metal foams (copper  
 588 and FeCrAlY—a steel alloy) fabricated with the rela-

Table 3  
Data for all materials used in performance comparison

| Material                                      | $H$ [mm] | Porosity         | Pore size [mm] | $U$ [m/s]   | $h$ [W/m <sup>2</sup> K] | $Re_H$      | $f$       | $Nu_H$   | $Nu/f$   | $Nu/f^{1/3}$ |
|---|----------|------------------|----------------|---|--------------------------|-------------|-----------|----------|----------|--------------|
| Brazed copper wire screens                    | 10       | 0.69–0.80        |                | 0.93–7.8  | 170–703                  | 685–7000    | 5–15      | 70.6–500 | 8–37.4   | 35.3–144     |
| Sintered FeCrAlY foams                        | 12       | 0.822–0.917      | 1.0–3.0        | 2.2–14.2  | 130–477                  | 2000–11 000 | 4–80      | 57–217   | 1–28     | 22–120       |
| Sintered copper foams                         | 12       | 0.881–0.94       | 0.55–3.0       | 0.67–10   | 77–728                   | 550–8200    | 13–88     | 35–332   | 0.4–20   | 20–141       |
| Lattice-frame materials (aluminum alloy LM25) | 12       | 0.938            | 12.7–14.7      | 1.84–21.4   | 125–482                  | 1500–18 000 | 0.61      | 57–220   | 93–360   | 67–259       |
| LFMs (polycarbonate)                          |          |                  |                |   |                          |             |           | 30–110   | 47–180   | 35–129       |
| Kagomé (BeCu)                                 | 12       | 0.926–0.971      | 12.2–14.7      | 1.54–31.5   | 109–563                  | 1200–27 000 | 0.3–0.64  | 50–257   | 120–700  | 58–383       |
| Kagomé (polycarbonate)                        |          |                  |                |   |                          |             |           | 25–154   | 70–420   | 29–230       |
| Aluminum foams                                | 9        | 0.92             | 1.6–3.9        | 1.1–5.4   | 115–400                  | 570–2800    | 6.1–13.5  | 39–140   | 4.8–15   | 16–77        |
| Packed beds (sintered bronze beads)           | 10.87    | 0.444            | 1.0–1.4        | $f = 307506/Re_H + 217.5$<br>$Nu_H = 0.0634Re_H^{1.0566}$ |                          | 500–20 000  | 221–833   | 45–12164 | 0.06–55  | 5–2013       |
| Packed beds (non-sintered steel beads)        | 10       | 0.4              | 1.2            | $f = 94938/Re_H + 155.4$<br>$Nu_H = 1.2503Re_H^{0.4732}$  |                          | 500–20 000  | 156–345   | 24–291   | 0.07–1.9 | 3.4–54       |
| Aluminum louvered fins                        | 4.45     |                  |                | 2–33  | 47.5–316                 | 600–10 000  | 0.06–0.4  | 8–53.5   | 80–1115  | 17–147       |
| Corrugated ducts                              |          |                  |                |   |                          | 250–2000    | 0.22–0.4  | 9–30     | 22.5–136 | 12–50        |
| Empty channel                                 |          | Laminar regime   |                | $f = 64/Re, Nu \sim \text{constant}$                      |                          | 100–2000    | 0.02–0.64 | 8.3      | 12–386   | 9–30         |
|   |          | Turbulent regime |                | $Nu = 0.023(Re)^{0.8} Pr^{0.4}$                           |                          | 2500–30 000 | 0.02–0.04 | 12–78.1  | 203–3900 | 35–228       |

589 tively cheap sintering route [23,24], aluminum foams  
590 made with the expensive investment casting route [25],  
591 packed beds with non-sintered steel beads and with  
592 sintered bronze beads [26], aluminum louver fin arrays  
593 [27], and corrugated ducts with sinusoidal wavy passages  
594 [28]; empty channel [29] is also included as datum.  
595 LFMs and Kagome structures are both periodic and  
596 highly porous ( $\epsilon \sim 0.9$ ), consisting a 3D network of  
597 cylindrical trusses. The porosity of the packed beds is  
598 low, about 0.4.

599 The design of a good heat exchanger demands a high  
600 heat transfer rate and a low mechanical pumping power  
601 needed to overcome fluid friction (pressure drop) and

602 move the fluid(s) through the heat exchanger. Hence,  
603 three aspects have been considered below: pressure drop,  
604 heat transfer rate, and the ratio of heat transfer rate to  
605 pressure drop, with the channel height selected as the  
606 characteristic length scale for each medium [24].

### 6.1. Pressure loss

607  
608 The comparison of overall pressure loss for different  
609 heat dissipation media is shown in Fig. 9a for a wide  
610 range of Reynolds numbers. Flow past packed beds  
611 experiences the highest drag. The typical flow resistance  
612 of foam materials is about two orders of magnitude

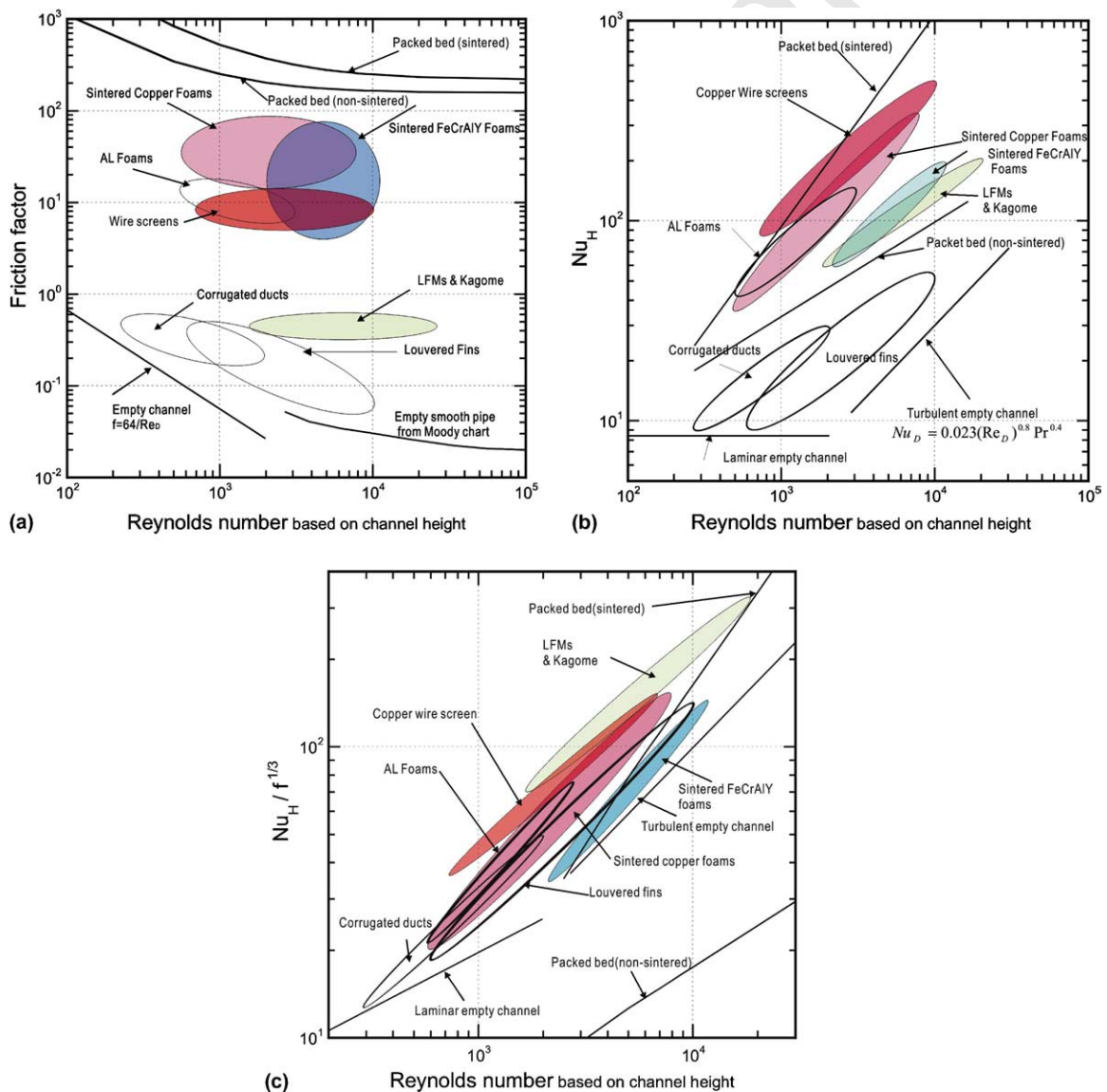


Fig. 9. Performance charts of different heat dissipation media: (a) friction factor; (b) heat transfer; (c) efficiency index  $Nu_H / f^{1/3}$ .

613 larger than that of the empty channel. It is also much  
614 larger than that of periodic materials such as textiles,  
615 Kagome structures and LFMs, even though the porosity  
616 of foams is high (comparable with Kagome structures  
617 and LFM but significantly larger than textiles), high-  
618 lighting the main difference between stochastic and  
619 periodic materials due to the difference in flow patterns.  
620 The flow resistance of LFMs and Kagome structures is  
621 about 10 times higher than that of an empty channel,  
622 but lower than that of wire screens. Both materials are  
623 periodic but have different porosities, with  $\varepsilon = 0.7\text{--}0.8$  for  
624 wire screens and  $\varepsilon \sim 0.9$  for LFMs and Kagome struc-  
625 tures. For periodic materials, porosity (as well as pore  
626 size) is the main characteristic dictating pressure loss.  
627 The selection of flow direction relative to pore topology  
628 is also important as discussed in Section 4.

## 629 6.2. Heat transfer

630 Fig. 9b compares the heat transfer performance of  
631 different heat dissipation media. Copper wire screens,  
632 copper foams, aluminum foams and packed beds with  
633 sintered bronze beads outperform corrugated ducts and  
634 louvered fins. Heat dissipation in the former group is  
635 contributed by both forced convection and conduction  
636 through the network of solid ligaments, whereas that in  
637 the second group depends mainly on the change in flow  
638 patterns caused by augment heat transfer surfaces. The  
639 copper wire screens tested in this study have porosities  
640 close to the optimal level ( $\varepsilon \approx 0.75$ ) that corresponds to  
641 the optimal combination of forced convection and solid  
642 conduction. Because of high porosity ( $\varepsilon > 0.9$ ) of foams,  
643 the contribution of solid conduction to the overall heat  
644 transfer is not as significant as that due to forced con-  
645 vection. This explains why there is no considerable dif-  
646 ference in terms of Nusselt number between foams made  
647 with high conductivity materials (copper and aluminum)  
648 and low conductivity materials (steel alloy). For packed  
649 beds, the high thermal contact resistance amongst non-  
650 sintered particles causes significantly inferior overall  
651 heat transfer performance to that of sintered particles.

## 652 6.3. Thermal efficiency

653 To compare the overall performance of different heat  
654 dissipation media, a thermal efficiency index defined  
655 using the average Nusselt number  $Nu_H$  and the friction  
656 factor  $f$  based on channel height will be used. Traditi-  
657 onally, this is done using the empirical index  $Nu_H/f$ .  
658 Whist this index may be useful to rank the performance  
659 of a series of heat exchangers having different geomet-  
660 rical parameters but same topological configuration  
661 (e.g., different louver fin arrays, or metal foams with  
662 different pore sizes and porosities), it is not adequate to  
663 compare the performance of different classes of heat

664 exchangers. For example, amongst the heat dissipation  
665 media considered in this work, the empty channel and  
666 louvered fin arrays have the best overall performance  
667 due mainly to the low pressure loss. Although foams  
668 have higher heat transfer rate, they have the lowest  
669 efficiency index due to high flow resistance as a result of  
670 stochastic cellular morphology. In other words,  
671 according to this index, metal foams and copper textiles  
672 are inferior to an empty channel. Consequently, the  
673 adequacy of the above thermal efficiency index is ques-  
674 tionable, and a modified efficiency index is used below.

675 Since the pumping power  $Q$  is equal to pressure drop  
676  $\Delta p$  times the volumetric flow rate, dimensional analysis  
677 dictates that:

$$Q \sim \Delta p u L^3, \quad f \sim \frac{\Delta p}{u^2}, \quad Re \sim uL \quad (12)$$

and hence 679

$$Q \sim f Re^3 \quad (13)$$

681 Consequently, the thermal efficiency index can be  
682 introduced as

$$\text{Efficiency index} = Nu_H / f^{1/3} \quad (14)$$

684 Performance charts plotted using  $Nu_H / f^{1/3}$  as one axis  
685 and  $Re_H$  as another are shown in Fig. 9c for stochastic  
686 materials, periodic structures, packed beds, louvered  
687 fins, corrugated ducts and empty channel. Physically,  
688 these charts rank the heat transfer capabilities of these  
689 heat dissipation media at a *fixed* pumping power. Fig. 9c  
690 reveals that all the heat dissipation media considered in  
691 this paper are better heat exchangers than an empty  
692 channel, except for the packed bed with non-sintered  
693 metallic particles. Note also that, in the form-dominated  
694 regime ( $Re_H > 1000$ ), periodic materials (LFMs, Kag-  
695 ome structures and copper textiles) have superior ther-  
696 mal efficiency to other media, and their overall  
697 performance may be further enhanced by optimizing the  
698 topology and porosity.

## 699 7. Conclusions

700 The overall pressure drop and heat transfer of brazed  
701 copper textile meshes have been experimentally investi-  
702 gated under steady-state forced air convection condi-  
703 tions. Prototype sandwiches with different topological  
704 configurations were tested along different flow orienta-  
705 tions, with uniform heat flux boundary condition im-  
706 posed.

707 For the range of Reynolds numbers considered, fluid  
708 flow in all textile meshes is form dominated: the friction  
709 factor in all cases is independent of the coolant velocity.  
710 The friction factor based on the unit pore size depends  
711 mainly on the open area ratio. If channel height is

712 chosen as the length scale, then the friction factor is also  
713 a function of pore size and flow direction.

714 The transfer of heat across the meshes depends on  
715 two competing mechanisms: solid conduction and  
716 forced convection. At a given Reynolds number,  
717 porosity and surface area density are two key param-  
718 eters controlling heat transfer. At a given porosity, the  
719 heat dissipation rate increases as the surface area density  
720 is increased. With increasing porosity, conduction de-  
721 creases while convection increases. Consequently, for a  
722 fixed surface area density, there exists an optimal  
723 porosity for maximum heat dissipation. For the copper  
724 textiles studied, this optimal porosity is about 0.75.

725 Performance charts are presented to compare copper  
726 textiles with selected heat dissipation media including  
727 metal foams, Kagome structures, lattice-frame materi-  
728 als, packed beds, corrugated ducts and louvered fins.  
729 Thermally, the copper textiles are as good as the sto-  
730 chastic metal foams, both having large surface area  
731 densities. However, the pumping power required is sig-  
732 nificantly lower for the textiles, because the periodic  
733 topology can be selected according to performance  
734 expectations: their overall thermal efficiency is about  
735 three times larger than that of copper foams. Significant  
736 opportunities exist to maximize the heat transfer per-  
737 formance of periodic cellular metals by varying the pore  
738 fraction, anisotropy of the pores and metallic alloy used.  
739 For multi-functional applications, further optimization  
740 requires simultaneous consideration of their thermal and  
741 structural properties.

## 742 Acknowledgements

743 We would like to thank Dr. D. J. Sypeck for his help  
744 in making two of the samples (S-1 and S-2) referred to in  
745 this work. The work was supported by the U.S. Office of  
746 Naval Research through ONR/ONRIFO grant number  
747 N000140110271 and ONR grant number  
748 N000140010342, and by the U.K. Engineering and  
749 Physical Sciences Research Council (EPSRC grant  
750 number EJA/U83).

## 751 Appendix A. Flow through an orifice plate

752 Consider the two-dimensional flow through an orifice  
753 plate as shown in Fig. 10. The orifice plate is introduced  
754 to model one unit cell of the periodic woven textile. Let  
755  $A_1$ ,  $A_2$  and  $A_3$  denote the cross-sectional area of the flow  
756 before (inlet), at and after (outlet) the orifice, and let  
757  $(u_1, u_2, u_3)$  and  $(p_1, p_2, p_3)$  denote the corresponding flow  
758 velocities and pressures. The continuity of mass dictates

$$\rho u_1 A_1 = \rho u_2 A_2 = \rho u_3 A_3 \quad (\text{A.1})$$

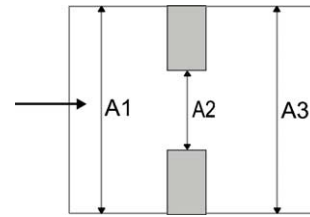


Fig. 10. Flow through an orifice plate.

when  $A_1 = A_2$ ,  $u_1 = u_3$ . Similarly, 760

$$\frac{u_2}{u_3} = \frac{A_3}{A_2} \quad (\text{A.2})$$

The momentum equation requires 762

$$P_2 A_3 + \rho u_2 u_2 A_2 = P_3 A_3 + \rho u_3 u_3 A_3 \quad (\text{A.3})$$

The pressure drop from location 2 to location 3 is 764

$$P_2 - P_3 = \rho u_3^2 - \rho u_2^2 \frac{A_2}{A_3} \quad (\text{A.4})$$

and the Bernoulli equation is given by 766

$$P_1 - P_2 = \frac{1}{2} \rho (u_2^2 - u_1^2) \quad (\text{A.5})$$

Combining Eqs. (A.1)–(A.5), one obtains the friction 768  
factor based on the unit cell size as 769

$$K_{\text{Cell}} = \frac{P_1 - P_3}{\rho u_1^2 / 2} = \left( \frac{1 - R_{\text{open}}}{R_{\text{open}}} \right)^2 \quad (\text{A.6})$$

where  $R_{\text{open}} = A_2/A_3$  is the open area ratio of the orifice 771  
plate. 772

## References 773

- [1] M.F. Ashby, A.G. Evans, N.F. Fleck, L.J. Gibson, J.W. 774  
Hutchinson, H.N.G. Wadley, *Metal Foams: A Design* 775  
*Guide*, Butterworth-Heinemann, 2000. 776
- [2] M. Kaviany, *Principles of Heat Transfer in Porous Media*, 777  
Springer, New York, 1995. 778
- [3] D.J. Sypeck, H.N.G. Wadley, Multifunctional microtruss 779  
laminates: textile synthesis and properties, *J. Mater. Res.* 780  
16 (2001) 890–897. 781
- [4] J. Tian, T. Kim, T.J. Lu, H.P. Hodson, D.J. Sypeck, 782  
H.N.G. Wadley, The effects of topology upon fluid-flow 783  
and heat-transfer within cellular copper structures, in: 784  
*Proceedings of 8th UK National Heat Transfer Confer-* 785  
*ence*, Oxford, 9–10 September 2003. 786
- [5] H.N.G. Wadley, *Cellular metals manufacturing*, *Adv. Eng.* 787  
*Mater.* 4 (2002) 726–733. 788
- [6] T.J. Lu, H.A. Stone, M.F. Ashby, Heat transfer in open- 789  
cell metal foams, *Acta Mater.* 46 (1998) 3619–3635. 790
- [7] A.G. Evans, J.W. Hutchinson, N.A. Fleck, M.F. Ashby, 791  
H.N.G. Wadley, The topological design of multifunctional 792  
cellular metals, *Prog. Mater. Sci.* 46 (2001) 309–327. 793

- 794 [8] D.R. Mumm, A.G. Evans, D.J. Sypeck, H.N.G. Wadley, On the performance of light weight metallic panels fabricated using textile technology, submitted.  
795  
796  
797 [9] J.C. Armour, J.N. Cannon, Fluid flow through woven screens, *AIChE J.* 14 (1968) 415–421.  
798  
799 [10] W.S. Chang, Porosity and effective thermal conductivity of wire screens, *ASME J. Heat Transfer* 112 (1990) 5–9.  
800  
801 [11] J.R. Sodr , J.A.R. Parise, Friction factor determination for flow through finite wire-mesh woven-screen matrices, *ASME J. Fluid Eng.* 119 (1997) 847–851.  
802  
803 [12] D. Mehta, M.A. Hawley, Wall effect in packed columns, *I&EC Process Des. Dev.* 8 (1969) 280–282.  
804  
805 [13] S. Ergun, Fluid flow through packed columns, *Chem. Eng. Prog.* 48 (1952) 89–94.  
806  
807 [14] F. Duprat, G. Lopez, Comparison of performance of heat regenerators: relation between heat transfer efficiency and pressure drop, *Int. J. Energy Res.* 25 (2001) 319–329.  
808  
809 [15] A. Ahmad, J. Saini, H. Varma, Effect of geometrical and thermo-physical characteristics of bed materials on the enhancement of thermal performance of packed-bed solar air heaters, *Energy Convers. Manage.* 36 (1995) 1185–1195.  
810  
811 [16] C.T. Hsu, K.W. Wong, P. Cheng, Effective stagnant thermal conductivity of wire screen, *J. Thermophys.* 10 (1996) 542–545.  
812  
813 [17] P. Jiang, M. Li, T.J. Lu, Z. Ren, X. Sun, Convection heat transfer in sintered porous plate channels, in: *Proceedings of 12th International Conference on Heat Transfer*, Grenoble, France, August 2002.  
814  
815 [18] T. Kim, A.J. Fuller, H.P. Hodson, T.J. Lu, An experimental study on thermal transport in lightweight metal foams at high Reynolds numbers, in: *Proceedings of International Symposium of Compact Heat Exchangers*, Grenoble, France, 2002, pp. 227–232.  
816  
817  
818  
819  
820  
821  
822  
823  
824  
825  
826
- [19] H.W. Coleman, W.G. Steele, *Experimentation and Uncertainty Analysis for Engineers*, second ed., John Wiley & Sons Inc., 1999. 827  
828  
829  
[20] T. Kim, C.Y. Zhao, T.J. Lu, H.P. Hodson, Convective heat dissipation with lattice-frame materials, *Mech. Mater.*, in press. 830  
831  
832  
[21] T. Kim, Fluid-flow and heat-transfer in a lattice-frame material, PhD Thesis, Department of Engineering, University of Cambridge, 2003. 833  
834  
835  
[22] F. Hoffmann, T.J. Lu, H.P. Hodson, Heat transfer performance of Kagome structures, in: *Proceedings of 8th UK National Heat Transfer Conference*, Oxford, 9–10 September 2003. 836  
837  
838  
839  
[23] C.Y. Zhao, Thermal transport in cellular metal foams with open cells, PhD Thesis, Department of Engineering, University of Cambridge, 2003. 840  
841  
842  
[24] C.Y. Zhao, T. Kim, T.J. Lu, H.P. Hodson, Thermal transport in high porosity cellular metal foams, *J. Thermophys. Heat Transfer*, in press. 843  
844  
845  
[25] S.Y. Kim, B.H. Kang, J.H. Kim, Forced convection from aluminum foams in an asymmetrically heated channel, *Int. J. Heat Mass Transfer* 44 (2001) 1451–1454. 846  
847  
848  
[26] P.X. Jiang, M. Li, T.J. Lu, Z. Ren, X. Sun, Convection heat transfer in sintered porous plate channels, in: *Proceedings of 12th International Conference on Heat Transfer*, Grenoble, France, August 2002. 849  
850  
851  
852  
[27] W.M. Kays, A.L. London, *Compact Heat Exchangers*, third ed., McGraw-Hill, Lond, 1984. 853  
854  
855  
[28] H. Blomerius, C. Holsken, N.K. Mitra, Numerical investigation of flow field and heat transfer in cross-corrugated ducts, *ASME J. Heat Transfer* 121 (1999) 314–321. 856  
857  
858  
[29] F.W. Dittus, L.M.K. Boelter, Heat transfer in automobile radiators of the tubular type, *Univ. California Publ. Eng.* 2 (1930) 443–461. 859  
860